www.sciencemag.org/cgi/content/full/341/6146/632/DC1

Supplementary Material for

A Quantum Many-Body Spin System in an Optical Lattice Clock

M. J. Martin,* M. Bishof, M. D. Swallows, X. Zhang, C. Benko, J. von-Stecher, A. V. Gorshkov, A. M. Rey,* Jun Ye*

*Corresponding author. E-mail: ye@jila.colorado.edu (J.Y.); mjmartin@caltech.edu (M.J.M.); arey@jilau1.colorado.edu (A.M.R.)

Published 9 August 2013, *Science* **341**, 632 (2013)
DOI: 10.1126/science.1236929

This PDF file includes:

Materials and Methods

Preparing the atomic sample

We load fermonic ^{87}Sr into a one-dimensional vertically oriented optical lattice via two-stage laser cooling, directly producing lattice-trapped samples with temperatures of 3–5 μK. The optical lattice is maintained near the magic wavelength (*31, 32*) for the ^{87}Sr $^1\mathrm{S}_0 \rightarrow {}^3\mathrm{P}_0$ clock transition. After further cooling and optical pumping into $^1\mathrm{S}_0$ $|F = 9/2, m_F = +9/2\rangle$, we obtain 5×10^3 nuclear spin polarized atoms concentrated mainly in a central region of several hundred disk-shaped lattice sites with typical trap frequencies as described in the text. The specific site occupancy distribution is calculated from the known MOT and lattice geometries. We determine the longitudinal temperature, T_Z, via sideband spectroscopy and the radial temperature, $T_\perp$, via Doppler spectroscopy (*21, 33*). With typical sample temperatures of $T_Z = 1 - 2$ μK, $T_\perp = 2 - 4$ μK, we find that for our trapping conditions the average density is $5(2) \times 10^{11}$ cm^{-3} for a sample consisting of 5×10^3 atoms. With the sample prepared as outlined above, we perform high-resolution spectroscopy on the $^1\mathrm{S}_0$ $|F = 9/2, m_F = +9/2\rangle \rightarrow {}^3\mathrm{P}_0$ $|F = 9/2, m_F = +9/2\rangle$ clock transition.

Contrast measurement

As described in the text, we measure Ramsey fringe contrast as a function of initial pulse area. For a first pulse of area θ_1, we allow the system to evolve for time τ. We then apply a final pulse of area $\pi/2$ and measure the resulting excitation fraction as a function of the optical phase of the second pulse relative to the first pulse. For $\tau \gtrsim 100$ ms, there is a significant additional random phase added due to the frequency fluctuations of the ultrastable clock laser. A given excitation fraction (p_i) measurement will yield $p_i = \mathcal{C} \sin^2(\Delta\phi_i)$, where $\mathcal{C}$ is the contrast and $\Delta\phi_i$ is the ith realization of the both

deterministically and randomly varied phase. By analyzing $\mathrm{Var}\,(p) = \mathcal{C}^2/8$, and assuming a uniform distribution of $\Delta\phi_i$, we obtain the contrast in a way that is insensitive to the laser noise.

Data analysis for spin noise measurement

We perform quadrature-dependent spin noise measurements as described in the text at a given target atom number $N_{\mathrm{tot}} = 1 \times 10^3$ or $N_{\mathrm{tot}} = 4 \times 10^3$. During the course of these measurements, we typically observe slow, systematic fluctuations of the atom number on the order of $\pm 10\%$ as we operate the experiment and measure spin noise over the course of $\sim$10 hours. In most instances, these fluctuations are negligible due to the normalization techniques we employ. However, the atomic spin noise depends directly on the atom number, and a slowly varying atom number could result in unintended systematic biases. Specifically, spin noise for the coherent spin state typically considered in optical clocks scales as $1/\sqrt{N_{\mathrm{tot}}}$. Thus, the deviations in atom number can cause variations on the order of $\pm 5\%$ in the measured spin noise. Ideally, these fluctuations are randomly distributed and should not result in interpretation as a false-positive for non-trivial spin-noise correlations. In the unlikely possibility that these fluctuations were correlated with a specific measurement quadrature, they could cause a spurious phase shift in the spin noise minimum. We thus take care to analyze the data in a way that is immune to this potential bias. In this supplement, we describe our process for removing the variability in the spin noise data due to a slowly fluctuating total atom number. In this way, we verify that the phase shifts measured in Fig. 4 are not manifestations of the "trivial" case, where the spin noise is described by a coherent spin state. Rather, we verify that the phase shift of the spin noise minimum is a direct result of the many-body interaction as described in the main text.

A given measurement of $\langle \hat{S}^z_{\rm tot}\rangle/N_{\rm tot}$ is accomplished by independently measuring $N_{e(g)}$, the number of atoms in the excited (ground) state after a single Ramsey experimental sequence, using standard electron shelving techniques. We determine its ith value, $\langle \hat{S}^z_{\rm tot}\rangle_i/N^i_{\rm tot}$, by measuring the ith value of $N_{e(g)}$ (which we denote as $N^i_{e(g)}$) and obtain

$$\langle \hat{S}^z_{\rm tot}\rangle_i/N^i_{\rm tot} = \frac{N^i_e}{N^i_e + N^i_g} - 1/2. \tag{S1}$$

From the jth set of measurements of $\langle \hat{S}^z_{\rm tot}\rangle$, denoted $\{\langle \hat{S}^z_{\rm tot}\rangle_1, \ldots, \langle \hat{S}^z_{\rm tot}\rangle_i, \ldots \langle \hat{S}^z_{\rm tot}\rangle_{n_j}\}_j$, we estimate $\sigma^2_j \equiv \langle (S^z_{\rm tot})^2\rangle/N^2_{\rm tot} - \langle \hat{S}^z_{\rm tot}\rangle^2/N^2_{\rm tot}$ using a pair variance, such that

$$\sigma^2_j = \frac{1}{2\left(n_j - 1\right)} \sum_{i=1}^{i=n_j} \left(\langle \hat{S}^z_{\rm tot}\rangle_{i+1} - \langle \hat{S}^z_{\rm tot}\rangle_i\right)^2. \tag{S2}$$

For white noise, the pair variance is a good estimator for the standard deviation (*34*), while remaining insensitive to noise processes that only manifest themselves on long time scales. The number of measurements in a set, n_j, was typically $n_j \simeq 80$. For a given measurement quadrature, we average the results of many such measurement sets to produce one experimental data point (*i.e.*, a data point in Fig. 4).

In order to maintain insensitivity to slow fluctuations in atom number between sets j and j', we consider the standard expression for quantum noise for the case of a coherent spin state, $\sigma_{\rm sql}$, which is expected in the absence of many-body interactions. The explicit goal is to remove any mechanism by which the trivial case—where the spin noise is described by $\sigma_{\rm sql}$—can mimic the many-body effect we predict from the theory. We calculate the jth value of $\sigma_{\rm sql}$ as

$$\left(\sigma^j_{\rm sql}\right)^2 = p_j\left(1 - p_j\right)/N^j_{\rm tot}, \tag{S3}$$

where $p_j = {\rm Mean}\left[\{N^1_e/\left(N^1_e + N^1_g\right), \ldots, N^i_e/\left(N^i_e + N^i_g\right), \ldots, N^{n_j}_e/\left(N^{n_j}_e + N^{n_j}_g\right)\}_j\right]$. We additionally consider a technical noise term, which represents the effect of intrinsic tech-

nical detection noise, given by Δs_j. This noise is characterized by a separate measurement. The detection noise accounts for 10% of the observed noise at typical low atom numbers, while at high atom number it is only $\sim 1\%$ of the observed noise, and is therefore negligible. It is quadrature-independent in all cases. From the σ_j^2, we subtract the atom-number-dependent $\left(\sigma_{\mathrm{sql}}^j\right)^2$ such that

$$\tilde{\sigma_j}^2 = \sigma_j^2 - \left(\sigma_{\mathrm{sql}}^j\right)^2 - \Delta s_j^2. \tag{S4}$$

Here, $\tilde{\sigma_j}^2$ represents only the effects of non-trivial spin noise and laser noise.

The many-body theory for a given measurement condition is calculated at fixed atom number. To facilitate comparison with the many body theory, we add a noise term back to $\tilde{\sigma_j}^2$ that corresponds to σ_{sql}^2 for the mean atom number over the entire data set, $\overline{\sigma_{\mathrm{sql}}^2}$. We emphasize that $\overline{\sigma_{\mathrm{sql}}^2}$ is a constant number, with no quadrature dependence. The many-body theoretical prediction is calculated based upon the same mean atom number used to calculate $\overline{\sigma_{\mathrm{sql}}^2}$. Ultimately, the net effect of this process is to remove the variability due to slow fluctuations in atom number, but to retain the part of the noise that departs from σ_{sql} due to both laser noise and many-body effects. As discussed in the text, we observe a phase shift of the minimum of the phase noise that is consistent with the many-body theory and indicative of correlated spin noise of the atom ensemble.

Linear response

As a complementary measurement of the density dependent frequency shift, we further probe the linear response dynamics of the system spectroscopically with a single weak pulse while varying δ. The pulse duration is $T_R = 500$ ms, and its area is $\Omega T_R \simeq 0.2\pi$. At this low excitation fraction, two-body losses can be ignored, and the mean-field analysis yields a density shift of the clock resonance given by $\Delta\nu_{\mathrm{LRR}} \simeq (C-\chi)N$, which agrees with the mean-field expression of the Ramsey frequency shift at small θ_1. In the experiment,

we observe a shift of 2.7 Hz for a modulation between $N_{\mathrm{High}} = 3 \times 10^3$ and $N_{\mathrm{Low}} = 1 \times 10^3$ (Fig. S1). We extract χ from the mean-field model described below (Eqns. S20 -S22) and find agreement at the 15% level, consistent with the atomic number distribution uncertainty.

Rabi spectroscopy

To further investigate interaction effects we also interrogate the system using Rabi spectroscopy. To allow high spectroscopic resolution of the many-body excitation spectra we reduce the atom-laser interaction energy, $\hbar\Omega$, to a level comparable to the many-body interaction energy and increased the pulse duration, T_R, so that $\Omega T_R = \pi$. In terms of the spin Hamiltonian, the presence of the probing pulse during the interrogation is equivalent to adding a transverse magnetic field-like term that does not commute with the Ising interactions, or to allowing for tunneling in the double-well BEC system thus giving rise to non-trivial quantum behavior (*35, 36*).

At the highest achievable densities in our experiment, we observe dramatic deviations in the Rabi lineshapes from ideal, single-particle lineshapes. By varying either the atom number or Ω (with $T_R = \pi/\Omega$), we change the ratio of the many-body interaction energy to $\hbar\Omega$. The resulting lineshapes are summarized in Fig. S2. At low atom number ($N_{\mathrm{tot}} \simeq 1 \times 10^3$) and with $T_R = 200$ ms, we observe a nearly ideal Rabi lineshape that becomes severely distorted with increasing density (Fig. S2A). Similarly, as we increase T_R, keeping $\Omega T_R = \pi$, we begin to see the onset of an interaction blockade mechanism (macroscopic self-trapping in the BEC context (*35*)) in concert with the distortion (Fig. S2B). At the largest $T_R = 750$ ms, we excite only 20% of the atoms into $|e\rangle$ and the line is approximately five times broader than the non-interacting lineshape.

Using the interaction parameters extracted via the Ramsey density shift and the linear

response measurements, we are able to theoretically reproduce all the observed lineshapes (theoretical curves shown in Fig. S2) using entirely a mean field approach (see Eqns. S20 -S22 below). Here, a full many-body treatment of the master equation is in agreement with the mean-field predictions.

Supplementary Text

Derivation of the spin Hamiltonian

The many-body Hamiltonian describing a nuclear spin-polarized ensemble of fermionic atoms with two accessible electronic states, g and e, which experience the same external potential $V_{ext}(\mathbf{R})$, can be expressed as (*37, 38*)

$$\begin{aligned}\hat{H} &= \sum_{\alpha}\int d^3\mathbf{R}\hat{\Psi}^{\dagger}_{\alpha}(\mathbf{R})\left(-\frac{\hbar^2}{2m}\nabla^2 + V_{ext}(\mathbf{R})\right)\hat{\Psi}_{\alpha}(\mathbf{R}) \\ &+\frac{4\pi\hbar^2 a^{-}_{eg}}{m}\int d^3\mathbf{R}\hat{\Psi}^{\dagger}_{e}(\mathbf{R})\hat{\Psi}_{e}(\mathbf{R})\hat{\Psi}^{\dagger}_{g}(\mathbf{R})\hat{\Psi}_{g}(\mathbf{R}) \\ &+\frac{3\pi\hbar^2}{m}\sum_{\alpha,\beta} b^3_{\alpha\beta}\int d^3\mathbf{R}\left[\left(\vec{\nabla}\hat{\Psi}^{\dagger}_{\alpha}\right)\hat{\Psi}^{\dagger}_{\beta} - \hat{\Psi}^{\dagger}_{\alpha}\left(\vec{\nabla}\hat{\Psi}^{\dagger}_{\beta}\right)\right]\cdot\left[\hat{\Psi}_{\beta}\left(\vec{\nabla}\hat{\Psi}_{\alpha}\right) - \left(\vec{\nabla}\hat{\Psi}_{\beta}\right)\hat{\Psi}_{\alpha}\right].\end{aligned} \tag{S5}$$

Here $\hat{\Psi}_{\alpha}(\mathbf{R})$ is a fermionic field operator at position $\mathbf{R}$ for atoms with mass m in electronic state $\alpha = g, e$. We have included only s-wave and p-wave channels, an assumption valid at μK temperatures. Since polarized fermions are in a symmetric nuclear-spin state, their s-wave interactions are characterized by only one scattering length a^{-}_{eg}, describing collisions between two atoms in the antisymmetric electronic state, $\frac{1}{\sqrt{2}}(|ge\rangle - |eg\rangle)$. The p-wave interactions can have three different scattering volumes b^3_{gg}, b^3_{ee}, and b^3_{eg}, associated with the three possible electronic symmetric states ($|gg\rangle$, $|ee\rangle$, and $\frac{1}{\sqrt{2}}(|ge\rangle + |eg\rangle)$, respectively. Note that here we have assumed no external laser field and have ignored the optical energy splitting since the number of atoms in the excited state remains fixed in the absence of driving terms.

In the experiment, $V_{ext}(\mathbf{R})$ is a deep 1D lattice along Z, which creates an array of two-dimensional discs and induces a weak harmonic radial (transverse) confinement with an angular frequency $\omega_R = 2\pi\nu_R$. The lattice confines the atoms to the lowest axial vibrational mode. We expand the field operator in a harmonic oscillator basis, $\hat{\Psi}_\alpha(\mathbf{R}) = \phi_0^Z(Z)\sum_{\mathbf{n}} \hat{c}_{\alpha\mathbf{n}}\phi_{n_X}(X)\phi_{n_Y}(Y)$, where ϕ_0^Z and ϕ_n are, respectively, the longitudinal and the transverse harmonic oscillator eigenmodes and $\hat{c}^\dagger_{\alpha\mathbf{n}}$ creates a fermion in mode $\mathbf{n} = (n_X, n_Y)$ and electronic state α. In this basis, $\hat{H}$ can be rewritten as (*18, 21*)

$$\begin{aligned}\hat{H} &= \sum_{\alpha,\mathbf{n}} E_{\mathbf{n}}\hat{n}_{\alpha\mathbf{n}} + \sum_{\alpha,\beta,\mathbf{n},\mathbf{n}',\mathbf{n}'',\mathbf{n}'''} \frac{\hbar}{4}\Big((1-\delta_{\alpha,\beta})uS_{\mathbf{n}\mathbf{n}'\mathbf{n}''\mathbf{n}'''} + v^{\alpha,\beta}P^{(2D)}_{\mathbf{n}\mathbf{n}'\mathbf{n}''\mathbf{n}'''}\Big)\hat{c}^\dagger_{\alpha\mathbf{n}}\hat{c}^\dagger_{\beta\mathbf{n}'}\hat{c}_{\beta\mathbf{n}''}\hat{c}_{\alpha\mathbf{n}'''},\\ u &= \sqrt{\omega_Z\omega_R}\frac{a^-_{eg}}{a^R_{ho}}, \qquad v^{\alpha,\beta} = \sqrt{\omega_Z\omega_R}\frac{b^3_{\alpha,\beta}}{{a^R_{ho}}^3} \end{aligned} \tag{S6}$$

$\delta_{\alpha,\beta}$ is a Kronecker delta function. Here, $a^R_{ho} = \sqrt{\hbar/(m\omega_R)}$ is the radial harmonic oscillator length, and $S_{\mathbf{n}\mathbf{n}'\mathbf{n}''\mathbf{n}'''}$ and $P_{\mathbf{n}\mathbf{n}'\mathbf{n}''\mathbf{n}'''}$ characterize s- and p-wave matrix elements respectively which depend on the harmonic oscillator modes and satisfy $S_{\mathbf{n}\mathbf{n}'\mathbf{n}''\mathbf{n}'''} = S_{\mathbf{n}\mathbf{n}'\mathbf{n}'''\mathbf{n}''} = S_{\mathbf{n}'\mathbf{n}\mathbf{n}''\mathbf{n}'''} = S_{\mathbf{n}'\mathbf{n}\mathbf{n}'''\mathbf{n}''}$ and $P_{\mathbf{n}\mathbf{n}'\mathbf{n}''\mathbf{n}'''} = -P_{\mathbf{n}\mathbf{n}'\mathbf{n}'''\mathbf{n}''} = -P_{\mathbf{n}'\mathbf{n}\mathbf{n}''\mathbf{n}'''} = P_{\mathbf{n}'\mathbf{n}\mathbf{n}'''\mathbf{n}''}$. $E_{\mathbf{n}}$ are single-particle energies in the trap.

For the quasi-2D geometry in consideration,

$$S_{\mathbf{n}\mathbf{n}'\mathbf{n}''\mathbf{n}'''} = s(n_X, n'_X, n''_X, n'''_X)s(n_Y, n'_Y, n''_Y, n'''_Y), \tag{S7}$$

$$P_{\mathbf{n}\mathbf{n}'\mathbf{n}''\mathbf{n}'''} = s(n_X, n'_X, n''_X, n'''_X)p(n_Y, n'_Y, n''_Y, n'''_Y) + p(n_X, n'_X, n''_X, n'''_X)s(n_Y, n'_Y, n''_Y, n'''_Y), \tag{S8}$$

$$s(n, n', n'', n''') \propto \frac{\int d\xi e^{-2\xi^2} H_n(\xi)H_{n'}(\xi)H_{n''}(\xi)H_{n'''}(\xi)d\xi}{\sqrt{2^{n+n'+n''+n'''}n!n'!n''!n'''!}}, \tag{S9}$$

$$p(n, n', n'', n''') \propto \tag{S10}$$
$$\frac{\int d\xi e^{-2\xi^2}\Big(\Big(\frac{d}{d\xi}H_n(\xi)\Big)H_{n'}(\xi) - H_n(\xi)\Big(\frac{d}{d\xi}H_{n'}(\xi)\Big)\Big)\Big(\Big(\frac{d}{d\xi}H_{n''}(\xi)\Big)H_{n'''}(\xi) - H_{n''}(\xi)\Big(\frac{d}{d\xi}H_{n'''}(\xi)\Big)\Big)}{\sqrt{2^{n+n'+n''+n'''}n!n'!n''!n'''!}}.$$

Here $H_n(x)$ are Hermite polynomials.

In Fig. S3 we show the mode dependence of the functions $p(n, n', n, n')$ and $s(n, n', n, n')$. While the $p(n, n', n, n')$ functions scale as $\sqrt{n + n'}$ and grow with increasing energy, as expected from $p-$ wave interactions, the $s(n, n', n, n')$ functions scale as $1/\sqrt{|n - n'|}$ and

thus decrease with increasing energy. However, note that both functions are weakly dependent on the mode coefficient and long ranged. In Fig. S4 we show the temperature dependence of the average $p-$wave interaction parameters $P_{\mathbf{nn'nn'}}$. There one can see that the average of $P_{\mathbf{nn'nn'}}$ is almost T independent in a quasi-2D geometry. This is expected because while the actual p-wave interactions for fixed density should increase linearly with T (*37*), the growth is compensated by the linear decrease with T of the density in a 2D harmonic trap. Fig. S4 also shows a histogram displaying the vibrational mode dependence of $P_{\mathbf{nn'nn'}}$ which is peaked about its average value. The histogram was computed at $T = 5\mu$K but it is almost T-independent. In Fig. S4 we assumed a Boltzmann distribution of the populated modes.

Under typical operating conditions, $\nu_R \sim 450$ Hz, the interaction energy is about two orders of magnitude weaker than the single-particle energy. Thus, at the leading order, only collision events that conserve the total single-particle energy need to be considered. Note that due to its non-separability and anharmonicity, the Gaussian profile of the transverse trapping potential suppresses those processes that do not conserve the number of particles per mode. In this case, for an initial state with at most one atom per mode ($|g\rangle$-polarized state), it is possible to reduce $\hat{H}$ to a spin-1/2 model.

$$\hat{H}^S/\hbar = \sum_{j\neq j'}^{N}[J^{\perp}_{\mathbf{n}_j,\mathbf{n}_{j'}}(\vec{S}_{\mathbf{n}_j}\cdot\vec{S}_{\mathbf{n}_{j'}}) + \chi_{\mathbf{n}_j,\mathbf{n}_{j'}}\hat{S}^z_{\mathbf{n}_j}\hat{S}^z_{\mathbf{n}_{j'}} + \frac{C_{\mathbf{n}_j,\mathbf{n}_{j'}}}{2}(\hat{S}^z_{\mathbf{n}_j}+\hat{S}^z_{\mathbf{n}'_j})]. \quad \text{(S11)}$$

Here $\vec{S}_{\mathbf{n}_j} = \frac{1}{2}\sum_{\alpha,\beta}\hat{c}^{\dagger}_{\alpha\mathbf{n}_j}\vec{\sigma}_{\alpha\beta}\hat{c}_{\beta\mathbf{n}_j}$, with $\sigma^{x,y,z}_{\alpha\beta}$ Pauli matrices. Constant terms have been dropped.

$$J^{\perp}_{\mathbf{n}_j,\mathbf{n}_{j'}} = \frac{V^{eg}_{\mathbf{n}_j,\mathbf{n}_{j'}} - U^{eg}_{\mathbf{n}_j,\mathbf{n}_{j'}}}{2}, \quad \chi_{\mathbf{n}_j,\mathbf{n}_{j'}} = \frac{V^{ee}_{\mathbf{n}_j,\mathbf{n}_{j'}} + V^{gg}_{\mathbf{n}_j,\mathbf{n}_{j'}} - 2V^{eg}_{\mathbf{n}_j,\mathbf{n}_{j'}}}{2}, \quad C_{\mathbf{n}_j,\mathbf{n}_{j'}} = \frac{(V^{ee}_{\mathbf{n}_j,\mathbf{n}_{j'}} - V^{gg}_{\mathbf{n}_j,\mathbf{n}_{j'}})}{2} \quad \text{(S12)}$$

The quantities

$$V^{\alpha\beta}_{\mathbf{n}_j,\mathbf{n}_{j'}} = v^{\alpha,\beta}P_{\mathbf{n}_j\mathbf{n}_{j'}\mathbf{n}_{j'}\mathbf{n}_j} \equiv v^{\alpha,\beta}P_{\mathbf{n}_j,\mathbf{n}_{j'}}, \quad U^{eg}_{\mathbf{n}_j,\mathbf{n}_{j'}} = uS_{\mathbf{n}_j\mathbf{n}_{j'}\mathbf{n}_{j'}\mathbf{n}_j} \equiv uS_{\mathbf{n}_j,\mathbf{n}_{j'}}, \quad \text{(S13)}$$

encapsulate the temperature dependence of the interactions. A further simplification of Eqn. S11 can be made thanks to the following considerations: (i) The atoms start in the totally symmetric manifold with $S = N/2$ since at time $t = 0$ all the atoms are polarized in the g state and the pulses that transfer atoms from g to e are collective. This condition is well satisfied in our experiment where the mode-dependent spread in Rabi frequency, $\Delta\Omega$, was measured to be small ($\Delta\Omega/\Omega \leq 0.1$), allowing on-resonance excitation probabilities of $\geq 98\%$; (ii) p-wave interactions are suppressed by the centrifugal barrier, and thus, at μK temperatures, U should in general dominate over V (although it must be said that the actual values of the s and p scattering parameters are not known); (iii) The p-wave matrix elements, $P_{\mathbf{n}_j,\mathbf{n}_{j'}}$, are functions which weakly dependent on $\mathbf{n}_j, \mathbf{n}_{j'}$ as explained above. All of these considerations generate an energy gap that prevents transitions between the $S = N/2$ and $S = N/2 - 1$ sectors. Consequently, to a very good approximation, the dynamics can be projected into the $S = N/2$ manifold with an effective Hamiltonian given by Eqn. 1 (which also contains single-particle terms arising from the optical driving field). We have omitted the term $\vec{S} \cdot \vec{S}$, which is a constant of motion when the dynamics is restricted to the $S = N/2$ manifold. $\chi_{\vec{\mathbf{n}}} = \frac{\sum_{j\neq j'} \chi_{n_j,n_{j'}}}{N(N-1)}$ and $C_{\vec{\mathbf{n}}} = \frac{\sum_{j\neq j'} C_{n_j,n_{j'}}}{N(N-1)}$ are mode-averaged quantities over the set of populated modes $\vec{\mathbf{n}}$. For a given realization, the modes that are populated are chosen according to Boltzmann distribution, and thermally-averaged observables are calculated by many iterations of this procedure. We note, however, that the thermal average of these quantities is highly independent of the temperature as shown in Fig. S4. We find therefore that the latter procedure converge very quickly to the solution obtained by just evolving one time the equations of motion with thermally averaged parameters. Due to this fact and to simplify the notation, we removed the subscript $\vec{\mathbf{n}}$ in the main text.

Decoherence and two-body losses – Exact treatment

The Hamiltonain formulation described above is valid only for a closed system. To account for losses due to inelastic e-e collisions, one needs to use instead a master equation:

$$\hbar\frac{d}{dt}\hat{\rho} = -\mathrm{i}[\hat{H},\hat{\rho}] + \mathcal{L}\hat{\rho}. \tag{S14}$$

Here $\hat{\rho}$ is the reduced density matrix operator of the many-body system. $\hat{H}$ is the Hamiltonian given by Eqn.1, and $\mathcal{L}$ is a Liouvillian that accounts for inelastic processes. Considering p-wave e-e losses and under the same assumption of frozen motional degrees of freedom, $\mathcal{L}$ is given by

$$\mathcal{L} \;=\; \sum_{j\neq j'}\frac{\hbar}{2}\Gamma_{\mathbf{n}_j,\mathbf{n}_{j'}}\left[2\hat{A}_{\mathbf{n}_j,\mathbf{n}_{j'}}\hat{\rho}(\hat{A}_{\mathbf{n}_j,\mathbf{n}_{j'}})^\dagger - (\hat{A}_{\mathbf{n}_j,\mathbf{n}_{j'}})^\dagger\hat{A}_{\mathbf{n}_j,\mathbf{n}_{j'}}\hat{\rho} - \hat{\rho}(\hat{A}_{\mathbf{n}_j,\mathbf{n}_{j'}})^\dagger\hat{A}_{\mathbf{n}_j,\mathbf{n}_{j'}}\right]. \tag{S15}$$

Here the jump operators are $\hat{A}_{\mathbf{n}_j,\mathbf{n}_{j'}} = \hat{c}_{e\mathbf{n}_j}\hat{c}_{e\mathbf{n}_{j'}}$ and $\Gamma_{\mathbf{n}_j,\mathbf{n}_{j'}} = \gamma^{ee}P_{\mathbf{n}_j\mathbf{n}_{j'}}$. The expression for γ is identical to $v^{e,e}$ up to the replacement of the p-wave elastic scattering volume by the inelastic one.

An important note is that there is no coherence between sectors of different atom numbers, and the master equation can be solved in a "block-diagonal" way (see Fig. 1). Specifically, if the system starts with N particles, we need to solve a series of differential equations for each of the subspaces with cascading atom numbers: first for N particles, next for $N-2$ particles, then for $N-4$ particles, etc. There are $\binom{N}{n} \equiv \frac{N!}{n!(N-n)!}$ different sectors with $N-n$ particles, $n = 0, 2 \ldots N$. In the case where the interaction parameters $\Gamma_{\mathbf{n}_j,\mathbf{n}_{j'}}$ are mode independent such that $\Gamma_{\mathbf{n}_j,\mathbf{n}_{j'}} \to \Gamma$, the dynamics in each of the $\mathcal{N} = N-n$ sectors is restricted to the collective Dicke states $|S = \mathcal{N}/2, M_\mathcal{N}\rangle \equiv |M_\mathcal{N}\rangle$. Moreover, each of the $\binom{N}{n}$ sectors behaves identically.

Let $\rho_\mathcal{N}$ be the density matrix for a single sector of $\mathcal{N}$ particles. Furthermore, let us assume that particles in $\rho_\mathcal{N}$ are numbered from 1 to $\mathcal{N}$ in such a way that atoms $\mathcal{N}+2$

and $\mathcal{N}+1$ are the ones that decay as one goes from $\rho_{\mathcal{N}+2}$ to $\rho_{\mathcal{N}}$. The resulting equations are

$$\frac{d}{dt}\rho_{\mathcal{N}} = -\frac{i}{\hbar}[H_{\mathcal{N}}, \rho_{\mathcal{N}}] - \frac{\Gamma}{2}\sum_{i<j}^{\mathcal{N}}(\hat{n}_{ei}\hat{n}_{ej}\rho_{\mathcal{N}} + \rho_{\mathcal{N}}\hat{n}_{ei}\hat{n}_{ej}) + \Gamma\binom{N-\mathcal{N}}{2}(\hat{c}_{e,\mathcal{N}+2}\hat{c}_{e,\mathcal{N}+1}\rho_{\mathcal{N}+2}\hat{c}^{\dagger}_{e,\mathcal{N}+1}\hat{c}^{\dagger}_{e,\mathcal{N}+2}), \tag{S16}$$

for $0 \leq \mathcal{N} \leq N$. In terms of spin operators,

$$\sum_{i<j}^{\mathcal{N}}\hat{n}_{ei}\hat{n}_{ej} = \frac{\mathcal{N}(\mathcal{N}-2)}{8} + \frac{\mathcal{N}-1}{2}\hat{S}^z + \frac{1}{2}(\hat{S}^z)^2, \tag{S17}$$

$$\langle M_{\mathcal{N}}|\hat{c}_{e,\mathcal{N}+2}\hat{c}_{e,\mathcal{N}+1}\rho_{\mathcal{N}+2}\hat{c}^{\dagger}_{e,\mathcal{N}+2}\hat{c}^{\dagger}_{e,\mathcal{N}+1}|M'_{\mathcal{N}}\rangle = \langle M_{\mathcal{N}+2}+2|\rho_{\mathcal{N}+2}|M'_{\mathcal{N}+2}+2\rangle \times\sqrt{\frac{\binom{\mathcal{N}}{M_{\mathcal{N}}+\mathcal{N}/2}\binom{\mathcal{N}}{M'_{\mathcal{N}}+\mathcal{N}/2}}{\binom{\mathcal{N}+2}{M_{\mathcal{N}}+\mathcal{N}/2+2}\binom{\mathcal{N}+2}{M'_{\mathcal{N}}+\mathcal{N}/2+2}}}. \tag{S18}$$

For $N \leq 50$, the above equations can be efficiently solved numerically. [1]

Mean-field treatment

Collective mean-field treatment

By a mean-field treatment we mean the approximation in which the collective spin operators are replaced by their expectation values. A simple and illuminating way to perform a mean-field treatment is to use the Schwinger-boson representation that maps spin operators to two-mode bosons (*39*). It represents the spin operators as

$$2\hat{S}^z = \hat{\Psi}^{\dagger}_1\hat{\Psi}_1 - \hat{\Psi}^{\dagger}_0\hat{\Psi}_0 \qquad \hat{S}^+ = \hat{\Psi}^{\dagger}_1\hat{\Psi}_0 \qquad \hat{S}^- = \hat{\Psi}^{\dagger}_0\hat{\Psi}_1, \tag{S19}$$

[1] At the highest operating densities, a cut-off of 50 atoms per lattice site is sufficient.

with $\hat{\Psi}_j$ a bosonic annihilation operator of mode $j = 0, 1$. In terms of Schwinger bosons, the collective spin model maps exactly to the Hamiltonian that describes a two-mode Bose-Einstein condensate (BEC), and it has been shown both theoretically (*23, 24, 40, 41*) and experimentally (*25–27*) that it gives rise to non-trivial many-body correlations and quantum-noise-squeezed states. It is also relevant in trapped-ion quantum simulation experiments (*10, 11, 42*). In the case where the two-modes (the 0 and 1 states) are identified as the left and right sites of a double-well bosonic system, the tunneling matrix element maps into Ω, a bias between the wells maps into δ, while V^{gg}, V^{ee} and V^{eg} map into the on-site interactions in the left and right wells and nearest-neighbor interactions, respectively. The mean-field approximation, which gives rise to the Gross-Pitaevskii equation, replaces the field operators $\hat{\Psi}_{1,0}$ with complex numbers, $\hat{\Psi}_{1,0} \rightarrow \Phi_{0,1}$. To deal with the lossy dynamics, it is necessary to express the equations of motion in terms of the density matrix, $\rho_{ij} \equiv \Phi_i^* \Phi_j$. The resulting equations are

$$\frac{\partial}{\partial t}\rho_{00} = -i\frac{\Omega}{2}(\rho_{10} - \rho_{01}), \tag{S20}$$

$$\frac{\partial}{\partial t}\rho_{11} = i\frac{\Omega}{2}(\rho_{10} - \rho_{01}) - \Gamma\rho_{11}^2, \tag{S21}$$

$$\frac{\partial}{\partial t}\rho_{10} = i\frac{\Omega}{2}(\rho_{11} - \rho_{00}) + i\left[-\delta + C(\rho_{11} + \rho_{00}) + \chi(\rho_{11} - \rho_{00}) + i\frac{\Gamma\rho_{11}}{2}\right]\rho_{10}, \tag{S22}$$

where $\rho_{01} = \rho_{10}^*$.

The mean-field treatment is expected to be valid in the regime $\sqrt{N}\sin[\theta_1]\chi t \ll 1$.

The evolution of the normalized contrast predicted by the mean field equations, after taking into account the Poissonian distribution over pancakes, is determined by a subtle competition between losses and dephasing. This competition emerges due to the fact that the dephasing depends on the excitation fraction and the latter decreases with time since losses only eliminate excited state atoms. Immediately after a $2\pi/3$ pulse for example, the contrast decay due to dephasing is very slow given that at this excitation fraction the

effective magnetic field induced by interactions is almost zero. The normalized contrast increases since we are dividing the contrast by the atom number, which decreases at a rate two times faster than the coherences (compare Eqns. S21 and S22). However, after some time, the excitation fraction decreases to a point at which the effective magnetic field is large enough that the dephasing compensates the factor of two faster decay rate of the atom number; and after this point the normalized contrast decreases monotonically.

"Multi-mode" mean-field treatment

In order to check the validity of the collective model, we have relaxed the collective mode approximation and derived "multi-mode" mean-field equations of motion. In those, the mode dependence of the p-wave interaction parameters is kept. To derive them, we assume that the reduced density matrix of the manybody system can be factorized as:

$$\rho \;=\; \prod_j \tilde{\rho}_{\vec{\mathbf{n}}_j} \qquad \tilde{\rho}_{\vec{\mathbf{n}}_j} \equiv \sum_{\alpha,\beta=e,g,0} \tilde{\rho}^j_{\alpha,\beta} |\alpha\rangle\langle\beta|. \tag{S23}$$

Here $\tilde{\rho}_{\vec{\mathbf{n}}_j}$ is the reduced density matrix of an atom in mode $\vec{\mathbf{n}}_j$, g, e label the two possible spin states of the atom, and 0 is the vacuum. Under the factorizable density matrix approximation, one can write closed equations of motion for $\tilde{\rho}^j_{\alpha,\beta}$. With the aim of dealing with long range interactions, it is better to write the equation of motion of the Fourier transformed quantities:

$$\rho_{\alpha\alpha}(k) \;=\; \sum_{j=1}^{N} e^{i\frac{2\pi jk}{N}} \tilde{\rho}^j_{\alpha,\alpha}, \tag{S24}$$

$$\rho_{eg}(k) \;=\; \sum_{j=1}^{N} e^{-i\frac{2\pi jk}{N}} \tilde{\rho}^j_{e,g} = \rho^*_{ge}(k), \tag{S25}$$

We note that, under the factorizable density matrix approximation, the equations of motion of $\tilde{\rho}^j_{\alpha,\beta}$ for $\alpha, \beta \in (e, g)$ are fully decoupled from the ones for $\tilde{\rho}^j_{\alpha,0}$ and $\tilde{\rho}^j_{0,\alpha}$, and thus we can ignore the latter.

The equations of motion derived in this way are general. They reduce to the collective mean-field equations, Eqns. (S20-S22), when the interaction parameters have only $k = k' = 0$ components. We have solved the equations of motion under various conditions and always found perfect agreement (at the 1% level) with the mean-field solutions obtained from the collective model. These observations validate the use of the latter for describing the dynamics.

Higher Order Corrections

The spin Hamiltonian neglects collision processes that do not preserve single-particle energy. However, collisions populating off-resonant states can still take place virtually and will introduce corrections to the spin model. To account for those, we split the Hilbert space into the resonant, Σ, and non-resonant, Υ, manifolds respectively, spanned by the states

$$|\Phi^{\Sigma}_{\vec{\sigma}_{\vec{n}}}\rangle = |\sigma_{\mathbf{n}_1}, \sigma_{\mathbf{n}_2}, \ldots, \sigma_{\mathbf{n}_N}\rangle, \quad E_0^{tot} \equiv \sum_{j=1}^{N} E_{\mathbf{n}_j}, \tag{S26}$$

$$|\Psi^{\Upsilon}_{\vec{\sigma}_{\vec{k}}}\rangle = |\sigma_{\mathbf{k}_1}, \sigma_{\mathbf{k}_2}, \ldots, \sigma_{\mathbf{k}_N}\rangle, \quad E_{\vec{\mathbf{k}}}^{tot} \equiv \sum_{j=1}^{N} E_{\mathbf{k}_j} \neq E_0^{tot}. \tag{S27}$$

These states are written in the occupation basis and $\sigma \in \{g, e\}$. In $|\sigma_{\mathbf{k}_j}\rangle$, the same mode $\mathbf{k}_j$ can also be occupied by both an e and a g atom simultaneously.

The spin Hamiltonian was obtained by just directly projecting the interaction part of the many-body Hamiltonian on Σ. An effective Hamiltonian that accounts for the leading order corrections generated by virtual occupation of non-resonant states can be derived by a simple generalization of the Schriffer-Wolf transformation (*43*):

$$\hat{H}^{\text{eff}}_{\vec{\mathbf{n}}} = \hat{H}^{S} + \hat{H}^{S_2}. \tag{S28}$$

Here, $\hat{H}^{S}$ is the spin model given by Eqn. S11. $\hat{H}^{S_2}$ can be obtained via second-order

perturbation theory as follows:

$$\langle \Phi^{\Sigma}_{\vec{\sigma}_{\vec{n}}} | \hat{H}^{S_2} | \Phi^{\Sigma}_{\vec{\sigma'}_{\vec{n}}} \rangle \;\; = \;\; -\sum_{\sigma_{\vec{k}}} \frac{\langle \Phi^{\Sigma}_{\vec{\sigma}_{\vec{n}}} | \hat{H} | \Psi^{\Upsilon}_{\vec{\sigma}_{\vec{k}}} \rangle \langle \Psi^{\Upsilon}_{\vec{\sigma}_{\vec{k}}} | \hat{H} | \Phi^{\Sigma}_{\vec{\sigma'}_{\vec{n}}} \rangle}{E^{tot}_{\tilde{\mathbf{k}}} - E^{tot}_{0}}, \tag{S29}$$

When $\hat{H}^{S_2}$ is written in terms of spin operators and is projected into the collective Dicke manifold, it gives rise to terms proportional to $\hat{S}^z$, $(\hat{S}^z)^2$ and $(\hat{S}^z)^3$ (we note that terms proportional to $(\hat{S}^z)^4$ vanish due to symmetry considerations). Among those corrections, the first two can be absorbed into the spin Hamiltonian given by Eqn. 1, and only the third one gives rise to additional corrections. The corrections in the Ramsey contrast decay arising from the cubic term are shown in Fig. S5. Similar higher-order interactions have been shown to introduce measurable corrections in bosonic systems (*44*).

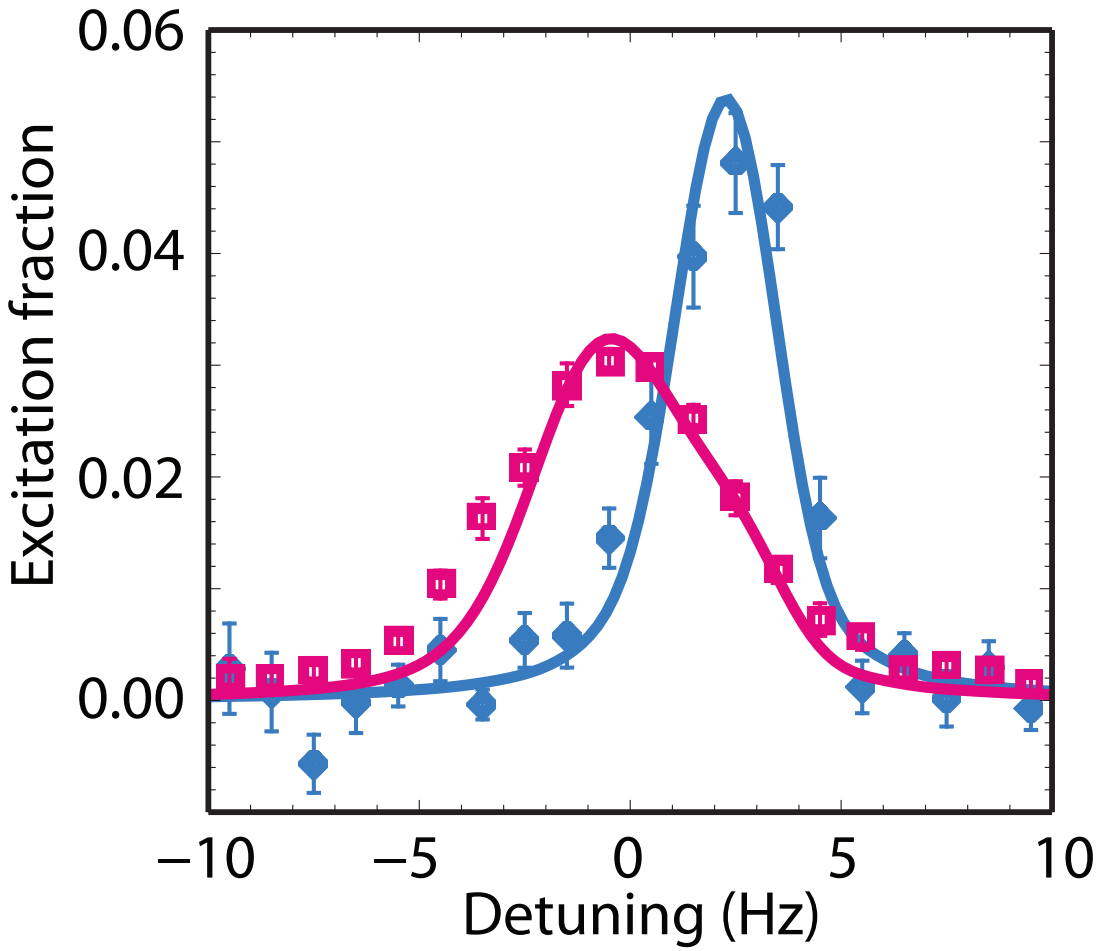

Figure S1: **linear response of the Rabi spectroscopic lineshapes under weak excitation** (pulse area $\theta_1 = 0.2\pi$). Here the pulse duration, $T_R = 500$ ms; the low atom number is $N_{\rm tot} \simeq 1500$ and high atom number is $N_{\rm tot} \simeq 4000$. The shift of the line center provides an independent verification of the model in the linear response regime.

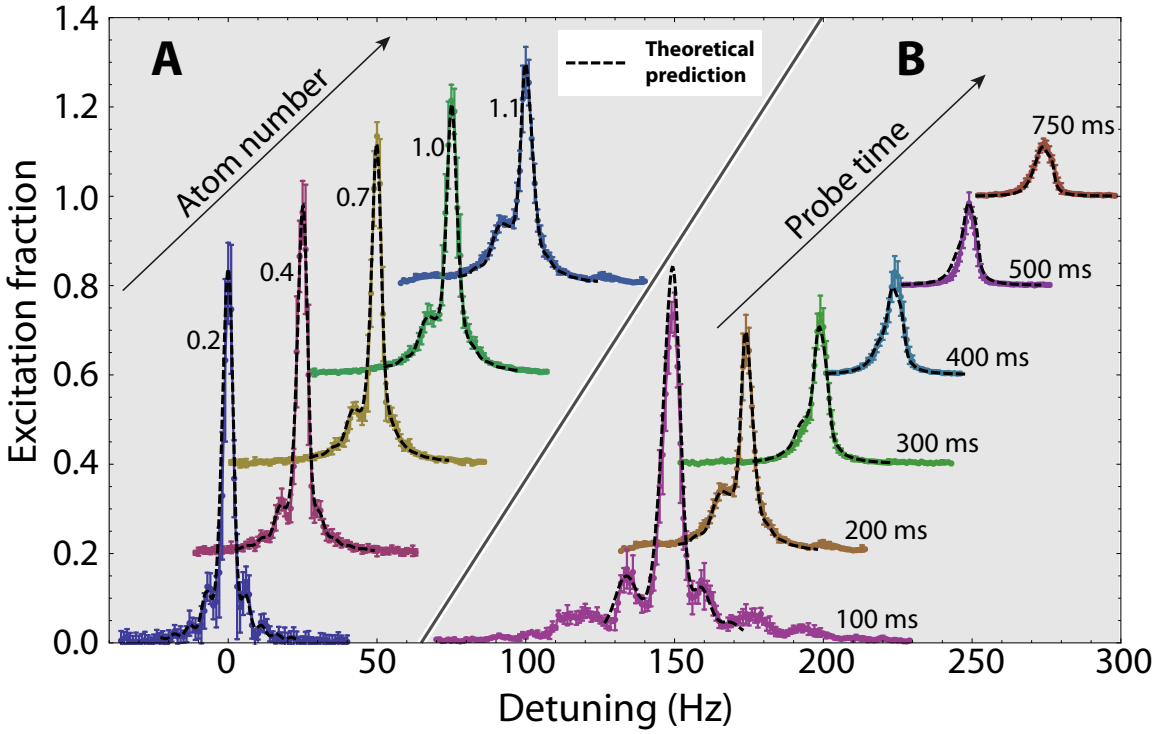

Figure S2: **Lineshape as a function of experimental parameters.** Each curve is a composite of multiple scans that have been centered atop one another and the data subsequently binned. The curves are offset in both the vertical and horizontal directions for visual clarity. **(A)** Lineshape as a function of density (normalized by $\rho_0 = 5(2) \times 10^{11}$ cm^{-3} the density obtained for 5×10^3 atoms), with a π-pulse time of 200 ms. **(B)** Lineshape for $\rho \simeq \rho_0$ as a function of probe time. In both **(A)** and **(B)**, theoretical curves, obtained with the mean-field treatment including loss, are shown as dashed black lines and agree well with the measurements.

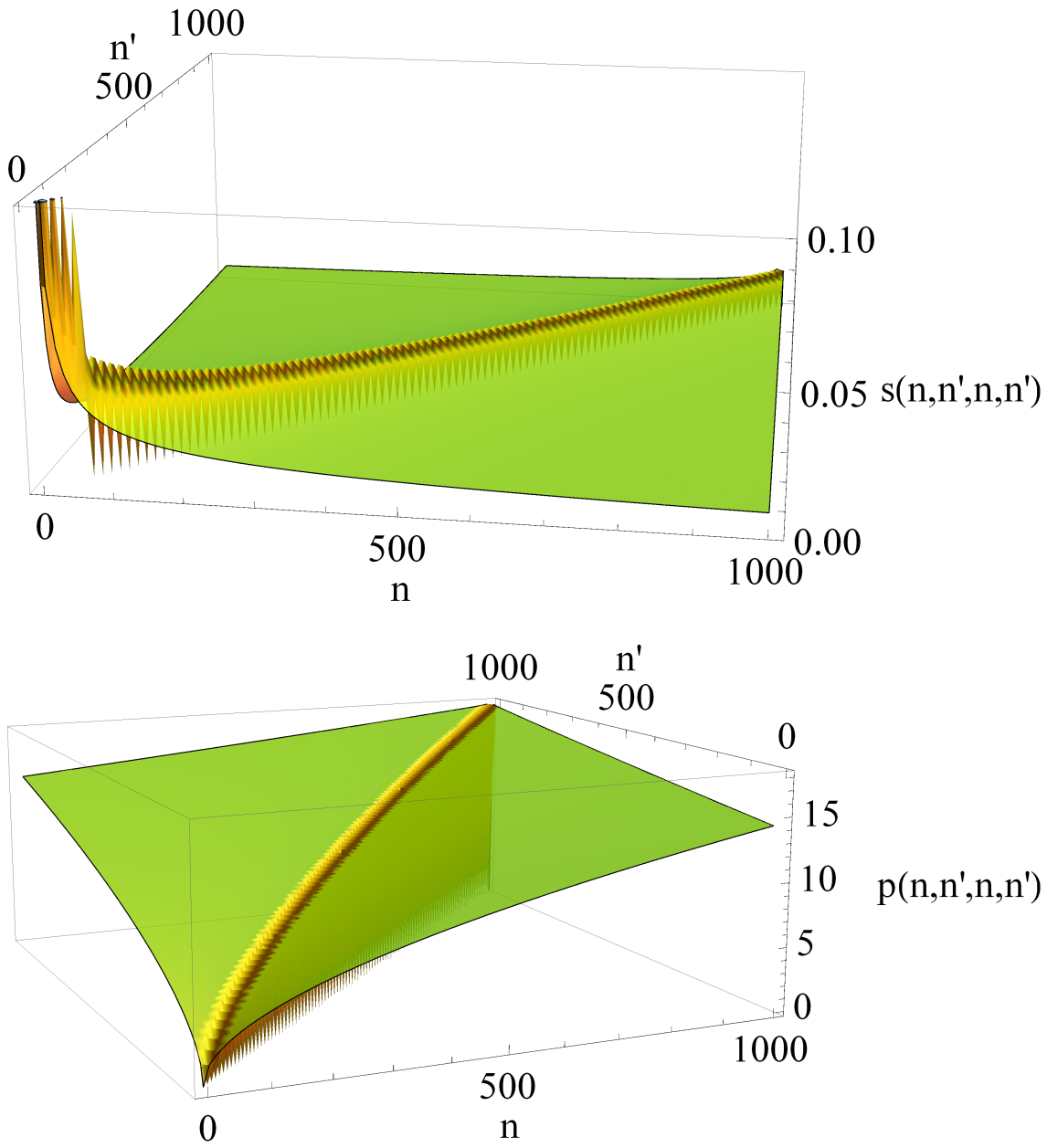

Figure S3: Mode dependence of the functions $p(n, n', n, n')$ and $s(n, n', n, n')$.

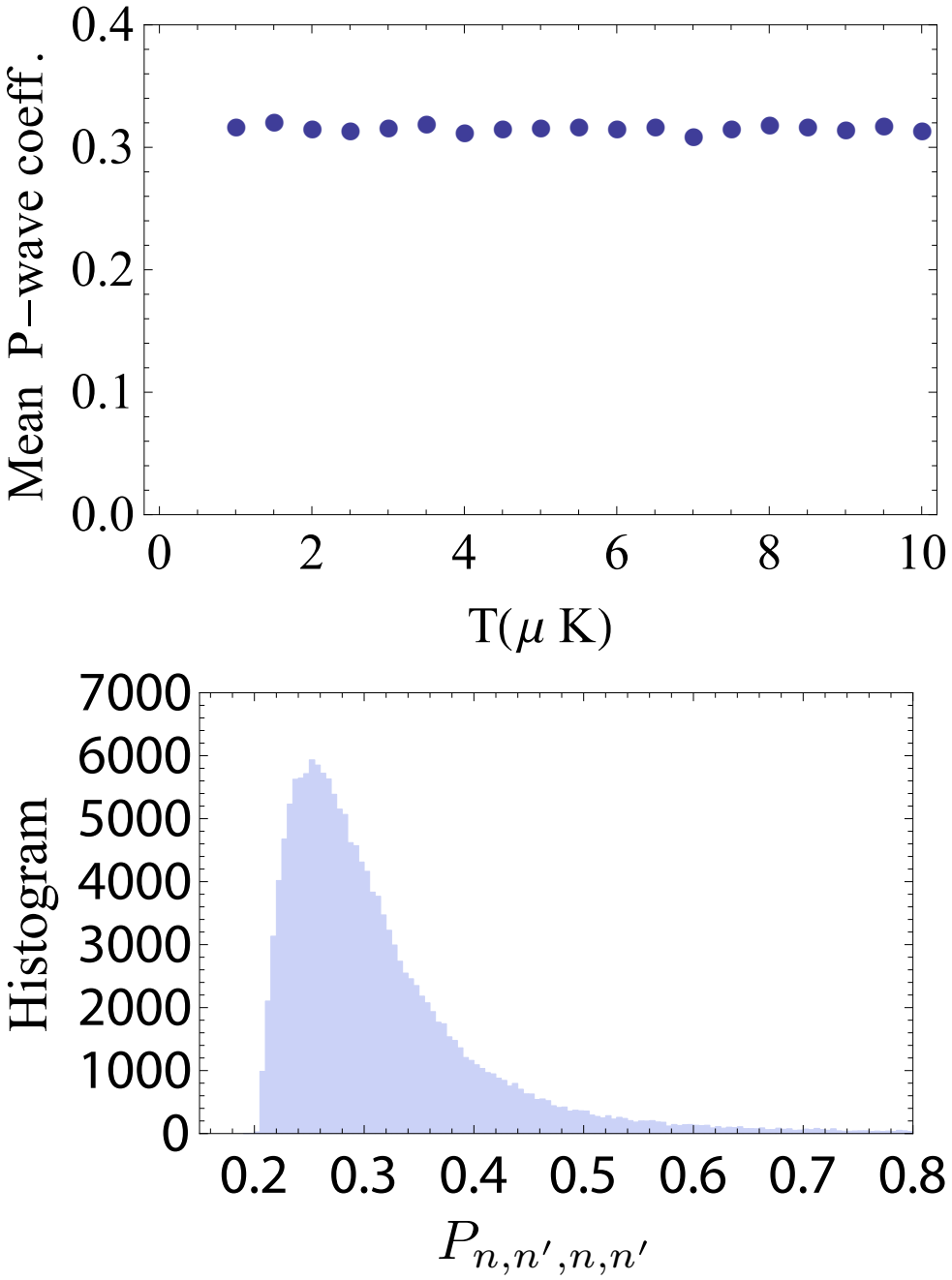

Figure S4: Top panel: Average value of the p-wave interactions vs Temperature. Bottom panel: Histogram of the vibrational mode dependence of $P_{\mathbf{nn'nn'}}$ at 5 μK. A Boltzmann distribution of the populated modes has been assumed.

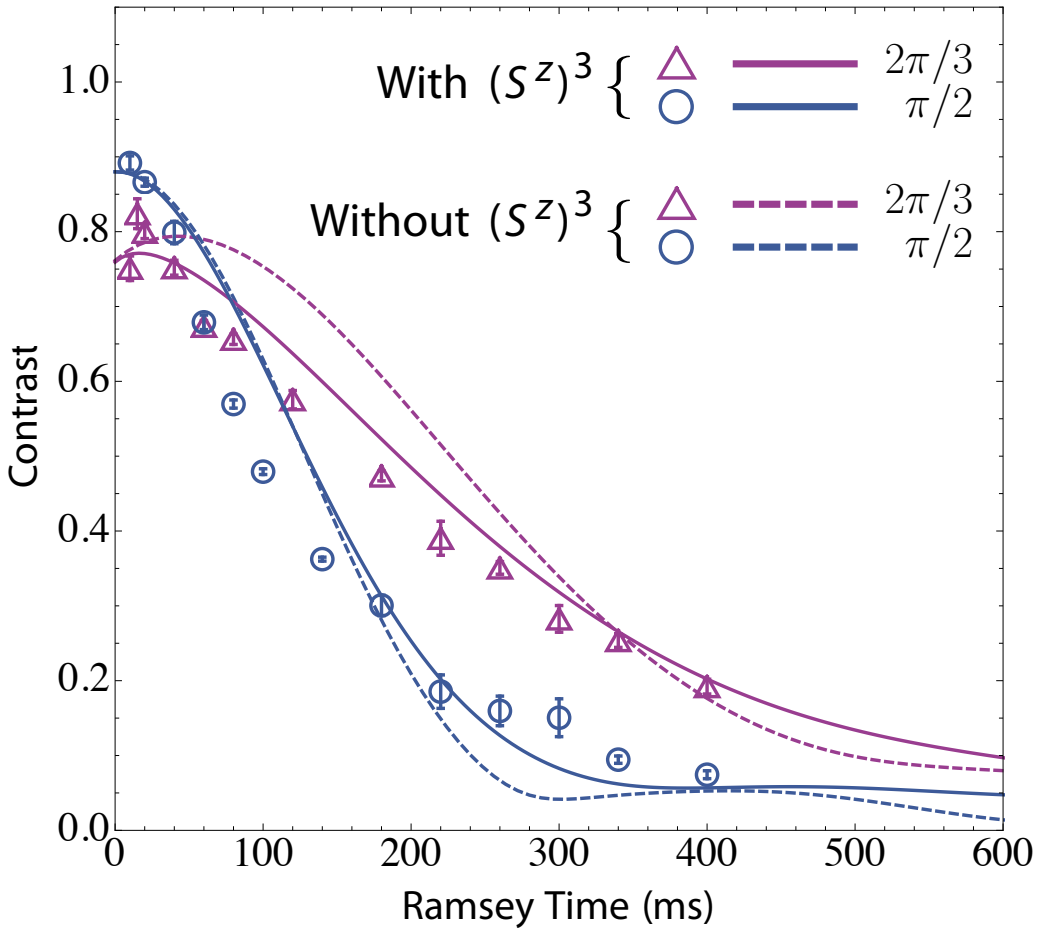

Figure S5: **Ramsey fringe contrast decay vs time for two different pulse areas.** The solid lines are the many-body fits using terms of order $\left(\hat{S}^z\right)^3$, and the dashed lines represent fits without these terms. These data are the same as in Fig. 3A of the main text, and were taken with $\nu_Z = 80$ kHz and $N_{\rm tot} = 4 \times 10^3$. Pulse areas are shown in the legend.

References and Notes

1. M. Greiner, O. Mandel, T. Esslinger, T. W. Hänsch, I. Bloch, Quantum phase transition from a superfluid to a Mott insulator in a gas of ultracold atoms. *Nature* **415**, 39–44 (2002). doi:10.1038/415039a Medline

2. I. Bloch, W. Zwerger, Many-body physics with ultracold gases. *Rev. Mod. Phys.* **80**, 885–964 (2008). doi:10.1103/RevModPhys.80.885

3. Y.-J. Lin, R. L. Compton, K. Jiménez-García, J. V. Porto, I. B. Spielman, Synthetic magnetic fields for ultracold neutral atoms. *Nature* **462**, 628–632 (2009). doi:10.1038/nature08609 Medline

4. G. B. Jo, Y. R. Lee, J. H. Choi, C. A. Christensen, T. H. Kim, J. H. Thywissen, D. E. Pritchard, W. Ketterle, Itinerant ferromagnetism in a Fermi gas of ultracold atoms. *Science* **325**, 1521–1524 (2009). doi:10.1126/science.1177112 Medline

5. S. Will, T. Best, U. Schneider, L. Hackermüller, D. S. Lühmann, I. Bloch, Time-resolved observation of coherent multi-body interactions in quantum phase revivals. *Nature* **465**, 197–201 (2010). doi:10.1038/nature09036 Medline

6. J. Simon, W. S. Bakr, R. Ma, M. E. Tai, P. M. Preiss, M. Greiner, Quantum simulation of antiferromagnetic spin chains in an optical lattice. *Nature* **472**, 307–312 (2011). doi:10.1038/nature09994 Medline

7. K. K. Ni, S. Ospelkaus, M. H. de Miranda, A. Pe'er, B. Neyenhuis, J. J. Zirbel, S. Kotochigova, P. S. Julienne, D. S. Jin, J. Ye, A high phase-space-density gas of polar molecules. *Science* **322**, 231–235 (2008). doi:10.1126/science.1163861 Medline

8. M. H. G. de Miranda, A. Chotia, B. Neyenhuis, D. Wang, G. Quéméner, S. Ospelkaus, J. L. Bohn, J. Ye, D. S. Jin, Controlling the quantum stereodynamics of ultracold bimolecular reactions. *Nat. Phys.* **7**, 502–507 (2011). doi:10.1038/nphys1939

9. A. Chotia, B. Neyenhuis, S. A. Moses, B. Yan, J. P. Covey, M. Foss-Feig, A. M. Rey, D. S. Jin, J. Ye, Long-lived dipolar molecules and Feshbach molecules in a 3D optical lattice. *Phys. Rev. Lett.* **108**, 080405 (2012). doi:10.1103/PhysRevLett.108.080405 Medline

10. K. Kim, M. S. Chang, S. Korenblit, R. Islam, E. E. Edwards, J. K. Freericks, G. D. Lin, L. M. Duan, C. Monroe, Quantum simulation of frustrated Ising spins with trapped ions. *Nature* **465**, 590–593 (2010). doi:10.1038/nature09071 Medline

11. J. W. Britton, B. C. Sawyer, A. C. Keith, C. C. Wang, J. K. Freericks, H. Uys, M. J. Biercuk, J. J. Bollinger, Engineered two-dimensional Ising interactions in a trapped-ion quantum simulator with hundreds of spins. *Nature* **484**, 489–492 (2012). doi:10.1038/nature10981 Medline

12. T. L. Nicholson, M. J. Martin, J. R. Williams, B. J. Bloom, M. Bishof, M. D. Swallows, S. L. Campbell, J. Ye, Comparison of two independent Sr optical clocks with 1×10^{-17} stability at 10^3 s. *Phys. Rev. Lett.* **109**, 230801 (2012). doi:10.1103/PhysRevLett.109.230801 Medline

13. A. D. Ludlow, T. Zelevinsky, G. K. Campbell, S. Blatt, M. M. Boyd, M. H. de Miranda, M. J. Martin, J. W. Thomsen, S. M. Foreman, J. Ye, T. M. Fortier, J. E. Stalnaker, S. A.

Diddams, Y. Le Coq, Z. W. Barber, N. Poli, N. D. Lemke, K. M. Beck, C. W. Oates, Sr lattice clock at 1 x 10^{-16} fractional uncertainty by remote optical evaluation with a Ca clock. *Science* **319**, 1805–1808 (2008). doi:10.1126/science.1153341 Medline

14. G. K. Campbell, M. M. Boyd, J. W. Thomsen, M. J. Martin, S. Blatt, M. D. Swallows, T. L. Nicholson, T. Fortier, C. W. Oates, S. A. Diddams, N. D. Lemke, P. Naidon, P. Julienne, J. Ye, A. D. Ludlow, Probing interactions between ultracold fermions. *Science* **324**, 360–363 (2009). doi:10.1126/science.1169724 Medline

15. A. M. Rey, A. V. Gorshkov, C. Rubbo, Many-body treatment of the collisional frequency shift in fermionic atoms. *Phys. Rev. Lett.* **103**, 260402 (2009). doi:10.1103/PhysRevLett.103.260402 Medline

16. K. Gibble, Decoherence and collisional frequency shifts of trapped bosons and fermions. *Phys. Rev. Lett.* **103**, 113202 (2009). doi:10.1103/PhysRevLett.103.113202 Medline

17. Z. H. Yu, C. J. Pethick, Clock shifts of optical transitions in ultracold atomic gases. *Phys. Rev. Lett.* **104**, 010801 (2010). doi:10.1103/PhysRevLett.104.010801 Medline

18. N. D. Lemke, J. von Stecher, J. A. Sherman, A. M. Rey, C. W. Oates, A. D. Ludlow, p-Wave cold collisions in an optical lattice clock. *Phys. Rev. Lett.* **107**, 103902 (2011). doi:10.1103/PhysRevLett.107.103902 Medline

19. A. Ludlow, N. D. Lemke, J. A. Sherman, C. W. Oates, G. Quéméner, J. von Stecher, A. M. Rey, Cold-collision-shift cancellation and inelastic scattering in a Yb optical lattice clock. *Phys. Rev. A* **84**, 052724 (2011). doi:10.1103/PhysRevA.84.052724

20. M. Bishof, M. J. Martin, M. D. Swallows, C. Benko, Y. Lin, G. Quéméner, A. M. Rey, J. Ye, Inelastic collisions and density-dependent excitation suppression in a ^{87}Sr optical lattice clock. *Phys. Rev. A* **84**, 052716 (2011). doi:10.1103/PhysRevA.84.052716

21. M. D. Swallows, M. Bishof, Y. Lin, S. Blatt, M. J. Martin, A. M. Rey, J. Ye, Suppression of collisional shifts in a strongly interacting lattice clock. *Science* **331**, 1043–1046 (2011). doi:10.1126/science.1196442 Medline

22. Materials and methods are available as supplementary materials on *Science* Online.

23. A. Sørensen, L. M. Duan, J. I. Cirac, P. Zoller, Many-particle entanglement with Bose-Einstein condensates. *Nature* **409**, 63–66 (2001). doi:10.1038/35051038 Medline

24. M. Kitagawa, M. Ueda, Squeezed spin states. *Phys. Rev. A* **47**, 5138–5143 (1993). doi:10.1103/PhysRevA.47.5138 Medline

25. J. Estève, C. Gross, A. Weller, S. Giovanazzi, M. K. Oberthaler, Squeezing and entanglement in a Bose-Einstein condensate. *Nature* **455**, 1216–1219 (2008). doi:10.1038/nature07332 Medline

26. C. Gross, T. Zibold, E. Nicklas, J. Estève, M. K. Oberthaler, Nonlinear atom interferometer surpasses classical precision limit. *Nature* **464**, 1165–1169 (2010). doi:10.1038/nature08919 Medline

27. B. Lücke, M. Scherer, J. Kruse, L. Pezzé, F. Deuretzbacher, P. Hyllus, O. Topic, J. Peise, W. Ertmer, J. Arlt, L. Santos, A. Smerzi, C. Klempt, Twin matter waves for interferometry

beyond the classical limit. *Science* **334**, 773–776 (2011). doi:10.1126/science.1208798 Medline

28. A. V. Gorshkov, M. Hermele, V. Gurarie, C. Xu, P. S. Julienne, J. Ye, P. Zoller, E. Demler, M. D. Lukin, A. M. Rey, Two-orbital SU(N) magnetism with ultracold alkaline-earth atoms. *Nat. Phys.* **6**, 289–295 (2010). doi:10.1038/nphys1535

29. C. Wu, J.-P. Hu, S.-C. Zhang, Exact SO(5) symmetry in the spin-3/2 fermionic system. *Phys. Rev. Lett.* **91**, 186402 (2003). doi:10.1103/PhysRevLett.91.186402 Medline

30. M. A. Cazalilla, A. F. Ho, M. Ueda, Ultracold gases of ytterbium: Ferromagnetism and Mott states in an SU(6) Fermi system. *New J. Phys.* **11**, 103033 (2009). doi:10.1088/1367-2630/11/10/103033

31. M. Takamoto, F.-L. Hong, R. Higashi, H. Katori, An optical lattice clock. *Nature* **435**, 321–324 (2005). doi:10.1038/nature03541 Medline

32. J. Ye, H. J. Kimble, H. Katori, Quantum state engineering and precision metrology using state-insensitive light traps. *Science* **320**, 1734–1738 (2008). doi:10.1126/science.1148259 Medline

33. S. Blatt, J. Thomsen, G. Campbell, A. Ludlow, M. Swallows, M. Martin, M. Boyd, J. Ye, Rabi spectroscopy and excitation inhomogeneity in a one-dimensional optical lattice clock. *Phys. Rev. A* **80**, 052703 (2009). doi:10.1103/PhysRevA.80.052703

34. J. Rutman, "Characterization of phase and frequency instabilities in precision frequency sources: Fifteen years of progress," in *Proceedings of the IEEE*, pp. 1048–1075 (1978).

35. A. Smerzi, S. Fantoni, S. Giovanazzi, S. R. Shenoy, Quantum coherent atomic tunneling between two trapped Bose-Einstein condensates. *Phys. Rev. Lett.* **79**, 4950–4953 (1997). doi:10.1103/PhysRevLett.79.4950

36. M. Albiez, R. Gati, J. Fölling, S. Hunsmann, M. Cristiani, M. K. Oberthaler, Direct observation of tunneling and nonlinear self-trapping in a single bosonic Josephson junction. *Phys. Rev. Lett.* **95**, 010402 (2005). doi:10.1103/PhysRevLett.95.010402 Medline

37. K. Kanjilal, D. Blume, Nondivergent pseudopotential treatment of spin-polarized fermions under one- and three-dimensional harmonic confinement. *Phys. Rev. A* **70**, 042709 (2004). doi:10.1103/PhysRevA.70.042709

38. K. R. A. Hazzard, A. V. Gorshkov, A. M. Rey, Spectroscopy of dipolar fermions in layered two-dimensional and three-dimensional lattices. *Phys. Rev. A* **84**, 033608 (2011). doi:10.1103/PhysRevA.84.033608

39. A. Auerbach, *Interacting Electrons and Quantum Magnetism* (Springer-Verlag, New York, 1994).

40. D. J. Wineland, J. J. Bollinger, W. M. Itano, F. L. Moore, D. J. Heinzen, Spin squeezing and reduced quantum noise in spectroscopy. *Phys. Rev. A* **46**, R6797–R6800 (1992). doi:10.1103/PhysRevA.46.R6797 Medline

41. M. Steel, M. Collett, Quantum state of two trapped Bose-Einstein condensates with a Josephson coupling. *Phys. Rev. A* **57**, 2920–2930 (1998). doi:10.1103/PhysRevA.57.2920

42. D. Porras, J. I. Cirac, Effective quantum spin systems with trapped ions. *Phys. Rev. Lett.* **92**, 207901 (2004). doi:10.1103/PhysRevLett.92.207901 Medline

43. L. M. Duan, E. Demler, M. D. Lukin, Controlling spin exchange interactions of ultracold atoms in optical lattices. *Phys. Rev. Lett.* **91**, 090402 (2003). doi:10.1103/PhysRevLett.91.090402 Medline

44. P. R. Johnson, E. Tiesinga, J. V. Porto, C. J. Williams, Effective three-body interactions of neutral bosons in optical lattices. *New J. Phys.* **11**, 093022 (2009). doi:10.1088/1367-2630/11/9/093022